On two-dimensional finite amplitude electro-convection in a dielectric liquid induced by a strong unipolar injection

Jian Wu[a1], Philippe Traoré[a1], Alberto T. Pérez[b], Pedro A. Vázquez[c]

[a] Département Fluide-Thermique-Combustion, Institut PPRIME, Université de Poitiers, Boulevard Pierre et Marie Curie, BP 30179, 86962 Futuroscope-Chasseneuil, France

[b] Departamento de Electrónica y Electromagnetismo, Universidad de Sevilla, Facultad de Física, Avenida Reina Mercedes s/n, 41012 Sevilla, Spain

[c] Departamento de Física Aplicada III, Universidad de Sevilla, ESI, Camino de los Descubrimientos s/n, 41092 Sevilla, Spain

Abstract

The hydrodynamic stability of a dielectric liquid subjected to strong unipolar injection is numerically investigated. We determined the linear criterion T_c (T being the electric Rayleigh number) and finite amplitude one T_f over a wide range of the mobility parameter M. A noticeable discrepancy is shown for T_f between our numerical prediction and the value predicted by stability analysis, which is due to the velocity field used in stability analysis. Recent studies revealed a transition of the flow structure from one cell to two with an increase in T. We demonstrate that this transition results in a new subcritical bifurcation.

Key words: Electro-convection; stability criteria; charge injection; numerical analysis; dielectric liquid.

[1]Corresponding authors. E-mail address: jian.wu@univ-poitiers.fr (Jian Wu). Tel.: +33 (0)5 49 49 69 34.

1. INTRODUCTION

Electro-convection induced by the unipolar charge injection into an insulating liquid is a fundamental problem in Electro-Hydro-Dynamics (EHD) [1,2]. The electro-chemical reaction at the interface between liquid and electrode gives rise to injection of ions [3], and the Coulomb force acting upon these injected free charges tends to destabilize the system and induce the flow motion. **This type of flow motion plays the center role in several industry applications, such as heat transfer enhancement [4,5] and flow control [6]. However, t**he inherent strong and complex nonlinear couplings in such a system make the problem difficult to analyze. For *homogeneous* and *autonomous* injection between two parallel planar electrodes, there are two basic features in the hydrodynamic stability. First, the hydrostatic state is potentially unstable. When the driving parameter exceeds a critical value, the instability sets in and flow motion takes place. Linear stability analysis shows that the linear criterion, which is a function of the electric Rayleigh number T, is highly dependent on the injection level C but independent on the dimensionless mobility parameter M [7]. Second, the linear bifurcation is subcritical and there exists a nonlinear instability criterion. This feature is due to the ion drift mechanism, which states that charge carriers migrate with a finite ionic velocity under the effect of electric field. The competition between the ionic velocity and the fluid velocity leads to the formation of the so-named charge void region [8]. Since the finite amplitude criterion is lower than the linear one, a hysteresis loop is established between them. The physical mechanism for the subcritical bifurcation was first deduced by Félici with a simplified hydraulic model of 2D rolls in the weak injection regime [9]. In that paper, the author proved that the maximum fluid velocity should be higher than the ionic velocity in order to sustain a stable electro-convective motion. The case of strong injection regime was later discussed by Atten and Lacroix [10]. Both the cellular patterns

of 2D rolls and 3D hexagonal cells were considered. With some assumptions, such as the infinite M number and the number of modes retained for the approximation of the velocity field, the nonlinear criteria for various injection levels were determined. For C=10, the nonlinear criteria for 2D rolls with one mode and two modes, 3D hexagonal cells with one mode were found to be about 125.0, 116.0 and 111.7, respectively [10]. These values have been widely compared with experimental and numerical results.

The subcritical bifurcation phenomenon has been qualitatively confirmed by experiments [11,12]. In [12], Atten and Lacroix reported the experimental results of the Space Charge Limited (SCL) regime ($C\rightarrow\infty$), and they illustrated the linear and finite amplitude criteria associated with the hysteresis loop with the current–voltage characteristics. Moreover, a hexagonal convective pattern was observed at the motion threshold [12,13], which is consistent with the theoretical prediction [10,13]. However, the theoretical predictions of the linear and finite amplitude stability criteria were 160.75 [7] and 110.0 [10], while experimental findings were about 110 and 90 respectively [12]. In addition, experimental observation revealed that the flow pattern at the motion threshold was not perfectly steady but always exhibited strong fluctuations around a well defined average. These discrepancies between theoretical analysis and experimental findings have not been well explained until now [14].

Since the numerical simulation can provide the dynamic of all basic fields, it is an efficient tool to gain additional insights into electro-convective phenomena. In simulating Coulomb-driven flows, the solving of charge density equation plays a central role [15,16]. The contribution of the molecular diffusion to charge transport is minimal [17], and thus it is often neglected. As a consequence the charge density equation is convection-dominated, and dedicated numerical algorithms are required to capture the steep gradient and simultaneously avoid unphysical

oscillations in the charge density distribution [18,19]. To date, several numerical methods have been developed to model Coulomb-driven flows, see the review paper [15]. A numerical solver is desirable to accurately reproduce both the linear and finite amplitude criteria. However, early attempts failed with the finite amplitude one because of the serious numerical diffusion resulting from the low order discretization schemes or coarse grids [8,19]. In [20], Chicón et al. developed a particle-in-cell (PIC) method for the charge density equation. To simplify the problem, the velocity field in [20] was not obtained by solving Navier-Stokes equations. Instead it was computed with an analytical expression, which was derived based on the assumption that the flow takes a form of 2D self-similar roll. We call this strategy of simulation as the Imposed Velocity Field (IVF) approach [19]. This is to be compared with the strategy of solving Navier-Stokes equations (SNS approach). Based on the IVF approach, Chicón et al. [20] found 121.4 for the finite amplitude criterion with C=10, which is close to 125, the value predicted by the nonlinear stability analysis. The case of C=10 has been commonly considered in numerical studies to represent a strong injection regime, all results listed below are with this strength. In [21], the same IVF strategy was utilized and the charge density equation was solved by the PIC method and a flux corrected transport (FCT) algorithm. The good agreement between the results obtained with the two methods was highlighted. Recently, the complete set of governing equations for EHD convection was successfully solved by several groups. In [22], a well tested direct numerical simulation code [23] was modified to include the electrical equations. For 2D cases with M=60, the obtained linear and finite amplitude criteria are about 162.0 and 110.0, respectively. In [24], Vázquez et al. extended their previous works by using a finite element (FEM) solver for Navier-Stokes equations. In [25], both 2D and 3D electro-convection were studied with the commercial software. However, only results of the linear stability criterion were reported in [24] and [25]. In [26], all equations were solved with a finite volume method (FVM),

and a total variation diminishing (TVD) scheme [27] was applied to the charge equation. For M=10, they found 155.64 and 107.5 for the linear and finite amplitude criteria, respectively. More recently, Vázquez and Castellanos developed a Discontinuous Galerkin FEM based algorithm [28]. For M=20, they found 108.7 for the finite amplitude criterion. In another recent paper [18], a comparison between the results obtained by IVF and SNS was performed. For M=40, the finite amplitude criteria obtained with IVF and SNS were about 121.0 and 109.0, respectively [18]. The most important results of the finite amplitude criterion are summarized in Table 1.

Table 1.Previous analytical and numerical predictions of the finite amplitude criterion for C=10.

Authors	Strategy	M	Results
Atten P, Lacroix J C [10]	Analytical, one-mode [a]	$+\infty$	125.0
	Analytical, two-mode [b]	$+\infty$	116.0
Chicón R et al. [20]	IVF, PIC, one-mode [a]	[5, 40], $+\infty$	121.4
Cerizza D [22]	SNS, 4th compact FD scheme	60	110.0
Traoré P, Pérez A T [26]	SNS, FVM TVD scheme	10	107.5
Vázquez P A, Castellanos A [28]	SNS, FEM Discontinuous Galerkin	20	108.7
Traoré P, Jian W [18]	IVF, FVM TVD scheme, one-mode [a]	40	121.0
	SNS, FVM TVD scheme		109.0

[a] and [b]: one-mode and two-mode mean the velocity formula used to approximate the two-dimensional rolls.

It is clear that previous numerical results covered a wide range of M. This is reasonable, since typical values of M for dielectric liquids vary in a wide range ($M \geq 3$) [2,17]. For example, the value of M for H^+ in ethanol is 4.1, while of Cl^- in chlorinated diphenyls in the range of [60, 475] [17]. In addition, the reported finite amplitude criteria are slightly different from one to the other. The difference may be due to numerical reasons (e.g. numerical diffusion and oscillations) since different numerical techniques were used. As will be demonstrated in this study, the relationship between the finite amplitude criterion and M also partially contributes to this difference. More

importantly, we are surprised to see that all results with the SNS approach, comparing to the IVF approach, are even farther away from the analytical values predicted by the stability analysis. It is well proved that the linear criterion is independent on M [7]. However, concerning the finite amplitude criterion, there is not a detailed study on its dependence on M. Using a FD scheme, Castellanos and Atten [19] found different values of the finite amplitude criterion for $M=60$ and $M\rightarrow\infty$ in the weak injection regime. However, their numerical approach was unable to resolve accurately the charge distribution, and their critical values were largely overestimated. On the other hand, Atten and Lacroix [10] called the attention on the possible dependence of the finite amplitude criterion on M in their conclusions. However, they did not address this issue in detail.

Numerical studies with strong injection have been extended to high values of T with the aim of determining the route to chaos or turbulence [24,25,26,28,29]. In [24], a transition of the flow structure from one convective cell to two cells with T=400 and $M\approx63.2$ was reported. Such a transition arises due to the nonlinear instability with high values of driving parameters, and it leads to a new bifurcation of the system. The same transition has been confirmed in later studies with different values of M [25,26,28,29]. In this paper we attempt to deepen the study by investigating the route that the two-cell flow structure returns to rest when T is decreased. The obtained results show a complete bifurcation diagram in the finite amplitude regime.

The main objective of this study is to determine the relationship between the finite amplitude criterion and M. The other goal is to extend the numerical bifurcation study to high electric Rayleigh numbers. The paper is organized as follows. In the next section the formulation of the physical problem is described. In Section 3, the numerical methods are explained. In Section 4 our numerical findings are reported and finally conclusions are given in the last section.

2. PROBLEM FORMULATION

2.1 Physical problem and governing equations

We consider a layer of perfectly insulating liquid confined between two parallel planar electrodes of length L and separated by a distance H. An electric potential difference ΔV is imposed between the two electrodes. The assumption of unipolar injection is made, i.e. only one species of ions with ionic mobility K are injected from the lower electrode into the bulk liquid. Following the theoretical studies [7,10] and other numerical ones [8,18-26], the injection is considered to be *homogeneous* and *autonomous*, which means that the density of injected charges at the emitter electrode always remains a constant value q_0, unaffected by the electric field and flow motion.

The fluid is assumed to be incompressible, Newtonian and linear isotropic. The classical EHD governing equations include the Navier-Stokes equations and a reduced set of Maxwell's equations in the electroquasistatics limit [30]. Taking as units H for length, ΔV for electric potential, ionic velocity scale $K\Delta V/H$ for velocity, $\rho K^2\Delta V^2/H^2$ for pressure, $H^2/K\Delta V$ for time and q_0 for charge density, the nondimensional governing equations read as [1,2]:

$$\nabla \cdot \vec{u} = 0, \tag{1}$$

$$\frac{\partial \vec{u}}{\partial t} + (\vec{u} \cdot \nabla)\vec{u} = -\nabla \tilde{p} + \frac{M^2}{T}\Delta \vec{u} + M^2 q\vec{E}, \tag{2}$$

$$\frac{\partial q}{\partial t} + \nabla \cdot \left(q\left(\vec{u} + \vec{E}\right)\right) = 0, \tag{3}$$

$$\Delta V = -q, \tag{4}$$

$$\vec{E} = -\nabla V, \tag{5}$$

where $\vec{u} \equiv [u, v]$ is the fluid velocity, $\vec{E} = [E_x, E_y]$ is the electric field, and q is the charge density. β represents the generalized pressure including the contribution from the electrostriction force term [2]. The diffusion term in the charge density equation Eqn. (3) has been neglected [17], thus ions are transported only by the fluid and drift velocities. The last term in Eqn. (2) represents the driving Coulomb force. Two dimensionless numbers appear in above equations,

$$T = \frac{\varepsilon \Delta V}{\rho \nu K}, \quad \text{and} \quad M = \frac{1}{K}\left(\frac{\varepsilon}{\rho}\right)^{1/2}.$$

where ρ is the liquid density, ε the permittivity; ν the kinematic viscosity. The electric Rayleigh number T represents the ratio between Coulomb force and viscous forces. The mobility parameter M is defined as the ratio of the so-called hydrodynamic mobility $\sqrt{\varepsilon/\rho}$ to the true mobility K. The meaning of M can also be interpreted in a different way. Assuming that the electrical energy $\varepsilon \vec{E}^2/2$ is entirely converted into the kinetic energy $\rho \vec{u}^2/2$, the vertical velocity component will be $v \sim (\varepsilon/\rho)^{1/2} E_y$. Then the ratio of the fluid velocity v and ion drift velocity KE_y scales as $v/KE_y \sim (\varepsilon/\rho)^{1/2}/K \equiv M$ [22,31]. This interpretation implies that the M parameter characterizes the influence of the injection induced flow motion on the transport and distribution of charges. For high values of M, charges tend to move mainly following the fluid velocity field.

2.2 Boundary and initial conditions

The boundary conditions associated to the problem are depicted on figure 1. The computational domain is confined in $0 \le x \le A = H/L$ and $0 \le y \le 1$. No-slip conditions for fluid velocity are applied on the two electrodes. Symmetric conditions are applied on lateral boundaries to follow the requirements adopted in stability analysis [8,19]. Two boundary

conditions are required to specify the ways in which charges are injected at the emitter electrode and removed from the collecting electrode [1]. The assumption of *homogeneous* and *autonomous* injection leads to $q = C$ at $y = 0$, where C is defined as $C = q_0 H^2 / \varepsilon \Delta V$ and it stands for the injection strength. Since the charge density equation is a first-order hyperbolic equation, no physical boundary condition is required at the collector.

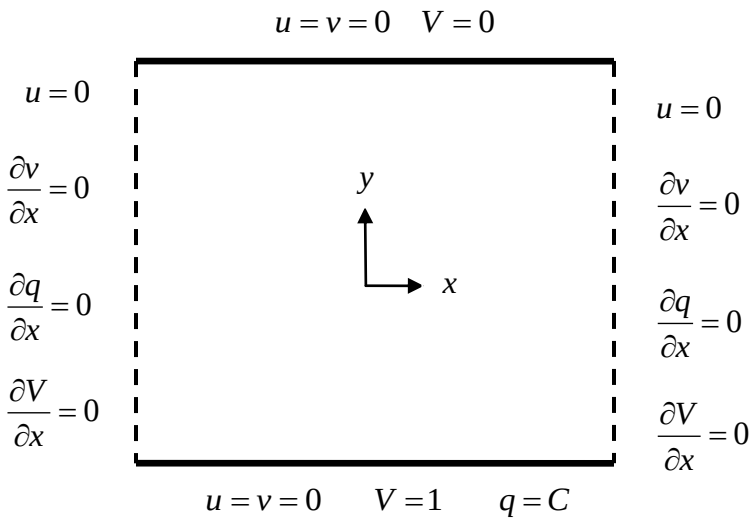

Fig. 1 Computational domain and numerical boundary conditions.

The governing equations (1)-(5) associated with these boundary conditions possess a hydrostatic solution, in which the fluid remains at rest while ions move from the emitter electrode to the collecting electrode with the drift velocity. The hydrostatics solution is expressed as [20]:

$$q(y) = \frac{a}{2} \frac{1}{\sqrt{y+b}} \text{ and } E(y) = a\sqrt{y+b}\,, \tag{6}$$

where a and b are two constants depending on C. For $C = 10$, a and b are 1.489 and 5.539×10^{-3}, respectively. The hydrostatic solution serves as the initial condition in the present study.

3. Numerical methods

The numerical procedure is based on a full and direct integration of Eqns. (1)-(5) with a 2^{nd} order in time and space finite volume method [32]. The computational domain is subdivided into non overlapping control volumes (CVs) where all variables are stored at the CV center in a collocated arrangement manner. In the numerical solver the Navier-Stokes equations are discretized with the 2^{nd} order central differencing (CD) scheme for both convective and diffusive fluxes. A 2^{nd} order semi-implicit three time levels scheme is used for the temporal discretization (Gear scheme). The SIMPLE algorithm [33] is undertaken for the velocity-pressure coupling and the Rhie-Chow momentum interpolation [34] is implemented to prevent the unphysical checker-boarder pressure field which may arise because of the collocated arrangement.

In simulating Coulomb-driven flows, the hyperbolic Eqn. (3) deserves some extra attention. In order to prevent spurious numerical oscillations and simultaneously preserve sharp gradients in the charge density distribution, the convective flux must be discretized using numerical schemes with some particular features. In this way the SMART scheme [35,36], which is one kind of TVD scheme, is adopted. The temporal discretization is also based on the Gear scheme. The interested readers may refer to [26,37] for additional numerical details.

When high-resolution schemes are applied to hyperbolic equations, a numerical boundary condition is required to update values of discrete cells on the outlet boundary. In our numerical implementation, the simple zero-order extrapolation is used at the collector. This condition can avoid the downstream information propagating back into the inner domain. For more details about the boundary condition treatment, please refer to [38].

4. RESULTS AND DISSCUSIONS

In this study, we restrict our attention to the strong injection case of C=10 that has been extensively discussed. The strong injection can be viewed as a good approximation of the SCL regime, for which some experiments have been performed [12,39,40]. To numerically reproduce the results of stability analysis, the aspect ratio of the domain A is set to 0.614, which corresponds to the half wavelength of the most unstable mode in this case [7]. The computational domain is discretized with a non-uniform grid consisting of 160×320 control volumes for all simulations. This grid is finally chosen based on a complete grid independence test. The grid is uniform in the x- direction and strongly non-uniform in the y- direction. In the y- direction, there are two sub-blocks separating at y=0.25. The bottom sub-block consists of 100 nodes, and the grid expands with a constant factor of 1.01. The finer grid size in the region close to the injecting electrode is desirable to capture the sharp variation in the charge density distribution in this region. The dimensionless time step is 10^{-3}.

4.1 Linear stability and flow structure

Similar to the classical Rayleigh-Bénard problem that a fluid layer is heated from below, the hydrostatic solution of Eqn. (6) is potentially unstable, implying a linear instability. This linear stability problem has been well analyzed [7,41]. Only for $T>T_c$ (T_c being the linear stability criterion), the external energy is sufficient to overcome the viscous friction and sustain the fluid motion. In addition, the bifurcation is subcritical. There exist a linear stability criterion and a nonlinear one, at which discontinuities occur in the electric current and velocity amplitude of fluid. The two criteria are associated with a hysteresis loop; see the schematic diagram of figure. 2. Note that T_c is closely related to C, and it is independent on M. For C = 10, T_c = 164.1 [7].

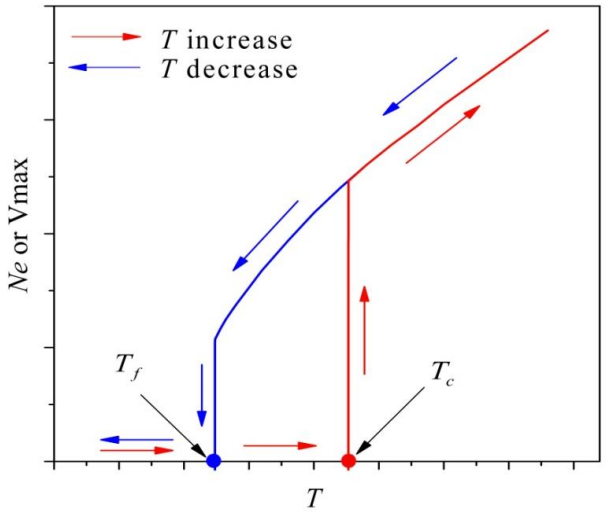

Fig. 2. Schematic diagram for the subcritical bifurcation in electro-convective problem. The electric Nusselt number *Ne* is defined as the ratio of the total electric current to the one without flow motion. Vmax represents the maximum velocity amplitude.

The subcritical nature of the electroconvective instability is an emblematic feature of Coulomb-driven flows between symmetrical electrodes. The physical reason leading to this particular bifurcation is related to the ion drift mechanism. Since a full derivation of the physical mechanism can be found in [1] and [2], we present here a brief description by combing the numerical results.

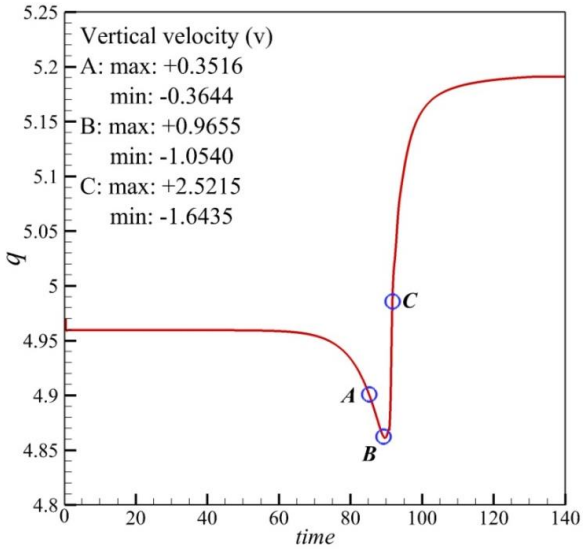

Fig. 3 Time history of charge density at a monitoring point (0.012, 0.02), T = 190, M = 10.

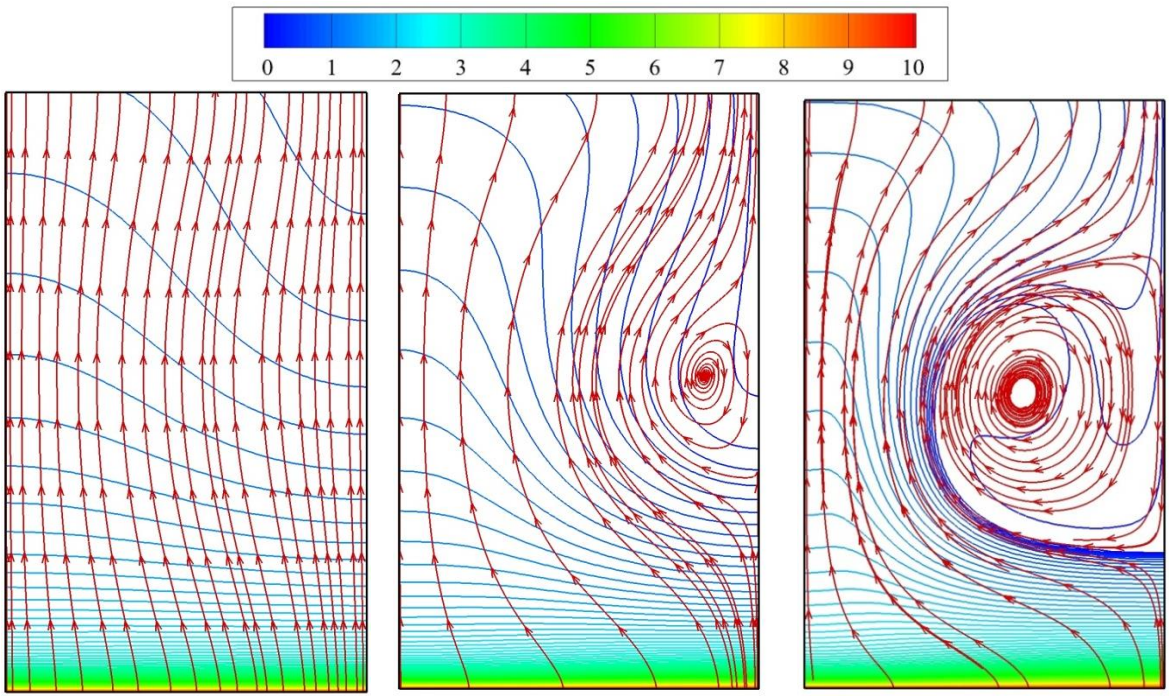

(a) (b) (c)

Fig. 4. Iso-lines of charge density distributions and stream traces based on $\varpi \overset{\omega}{u} + \overset{\omega}{E}$ for points (a) *A*, (b) *B* and (c) *C* of figure 3 to highlight the transport trajectories of charges.

In figure 3 we have plotted the time history of charge density at a monitoring point that is close to the emitter electrode. The charge density distribution and the stream traces of charges for three representative points (*A*, *B*, *C* on figure 3) are shown in figure 4. The stream traces are plotted with the full convective velocity $\varpi \overset{\omega}{u} + \overset{\omega}{E}$ for charge transport; see Eqn. (3). From these figures we can separate the whole formation process of the final steady motion into two stages. In the first stage, the flow velocity is small and grows smoothly in time. As shown in figure 4a, the weak flow motion gives rise to a non-uniform distribution of charge density and consequently a non-zero electric torque. Felici deduced that this driving electric torque is a concave function of the velocity amplitude [9]. In other words, once the fluid is put into motion, the driving electric torque tends to increase faster than the viscous effect, which will cause a new increase in the fluid velocity. Such a positive feedback mechanism explains the sustained growth of the fluid velocity

(i.e., the upward jump at T_c in figure 2). Once the downward velocity equals to the ionic velocity, the system enters into the second stage. At this stage, the electric torque is saturated while the fluid velocity continues to increase. More importantly a region strictly free of charges gradually forms. Since the downward fluid velocity in some regions is greater than the upward ionic velocity, electric charges cannot cross these regions. As shown in figure 4c, ions injected from the most right-hand side of the emitter electrode are mainly carried by the fluid field towards the opposite electrode [8,28]. Eqn. (3) can be rewritten as $\partial(1/q)/\partial t + (\vec{\omega}+\vec{E})\cdot\nabla(1/q)=1$, thus along the ion trajectory $d(1/q)/dt = 1 \Rightarrow q = q_0/(1+q_0 t)$ [19]. Two situations arise [42]: outside the void region, the charge density continuously decreases in limited time along the trajectory connecting the emitter and collecting electrodes. Inside the void region, charges follow closed trajectories (see figure 4c) and the charge density eventually becomes zero considering $\lim_{t\to\infty}(q_0/(1+q_0 t))=0$, implying that this region remains strictly free of charges. The appearance of non-charged region accounts for the subcritical behavior of the instability [8,17]. We especially noticed that the transition between the two stages takes place at point *B* located at the minimum of the curve *q* versus *time* (figure 3). At this point, the corresponding minimum value of downward velocity is -1.054, which is very close to 1.0, the ionic velocity scale.

We take *M*=10 as a representative example to describe the flow structure at final steady state. In the charge density distribution (figure 5a), we first observe that there is a sharp variation in the vertical direction, especially in the region close to the emitter electrode. In addition, a central region is almost free of charges ($q \to 0$). It should be noted that the void region is not closed but it allows for an open hole on the collecting electrode (see figure 6). The open hole is formed due to the strong Coulomb repulsion between ions [17,20]. In figure 5b, we observe an asymmetrical distribution of stream function, while with the IVF method the obtained distribution is usually

symmetric [18]. In the IVF methods, the velocity field is assumed to be self-similar, i.e. of the form $\varpi(x,y,t) = A(t)\varpi_0(x,y)$ [18-20]. The amplitude $A(t)$ is calculated averaging Eqn. (2) over one cell. Since $\int_{cell} \varpi_0(\varpi_0 \cdot \nabla)\varpi_0 dxdy = 0$ for any choice of ϖ_0, symmetric or not, this approach cannot give any dependence on *M*. This is the reason why IVF methods are not suitable to study the dependence of the finite amplitude criterion on *M*.

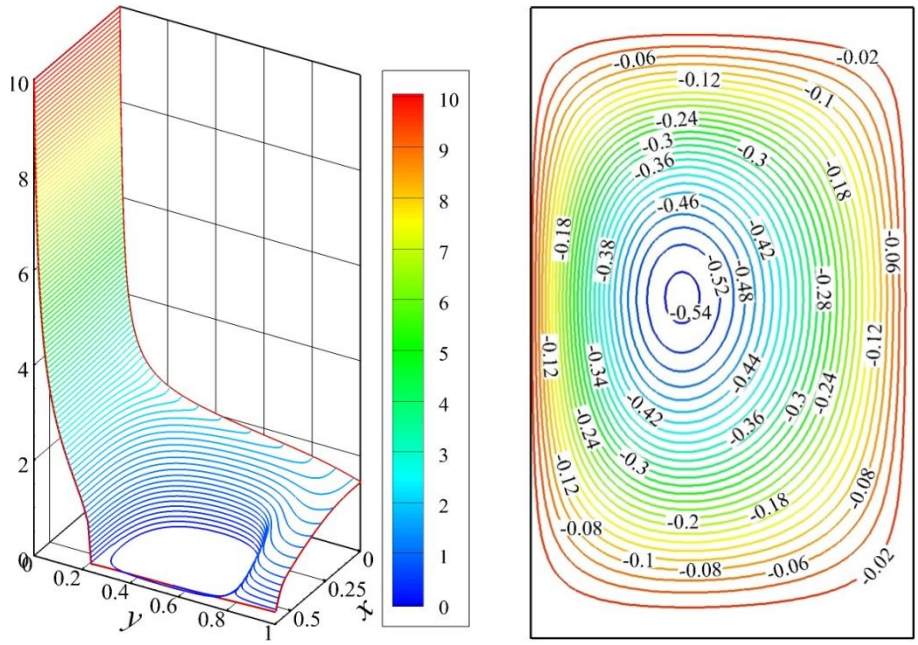

(a) (b)

Fig. 5 Steady convection for T = 190 and M = 10. Iso-contours of (a) charge density and (b) stream function.

In figure 6 we have displayed the curve *q=0.5* which materializes the boundary between the charged and non-charged regions at different *M*. The value of *q* in the void region is not strictly zero but with a fairly small value of order 10^{-5}~10^{-4}. This is due to the residual numerical diffusion induced by the numerical scheme which is impossible to cancel completely. In any case, the small non-zero value of *q* in the central region will not affect the overall behavior of the system and especially the value of the finite amplitude criterion. The choice of value *q*=0.5 is

arbitrary and corresponds to 5% of the total amount of injected charges. We have compared the separatrix curves represented by various values ranging from 0.1 to 0.9, and not much difference is observed. In figure 6, the curves for M = 20, 50, 100 and 200 are nearly indistinguishable. However, for M < 20, the results become M-dependent.

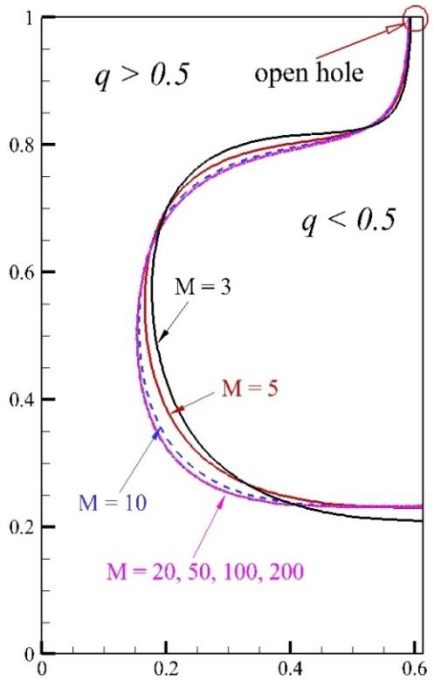

Fig.6 Distributions of charge density for T = 190 and various values of M. The region free of charges is highlighted by the area of q < 0.5.

In figure 7 we have plotted the longitudinal and vertical velocity profiles along the vertical and horizontal mid-sections (respectively x = 0.307 and y = 0.5). The same observations as figure 6 can be done concerning the M-dependency. In Table 2, we have listed the maximum vertical velocity, angular momentum and electric Nusselt number for the same value of T but with different values of M. The angular momentum (AM) stands for the strength of convective rolls, and it is defined as $AM = \int_{\text{domain}} (\vec{r} - \vec{r}_0) \times \vec{u} dS$, where $\vec{r}_0$ is the position vector of a given point. The electric Nusselt number (Ne) is defined as the ratio between the total electric current and the current without motion. Ne is similar to the classic Nusselt number in heat transfer, and it is

widely used to indicate the increase of electric current by the flow motion. According to this table we see that the results for all cases where $M > 20$ only vary from 0 to 0.05% according to the variations in *AM* and *Ne*. However, the changes are more visible for lower values of *M*, which manifests a clear *M*-dependency.

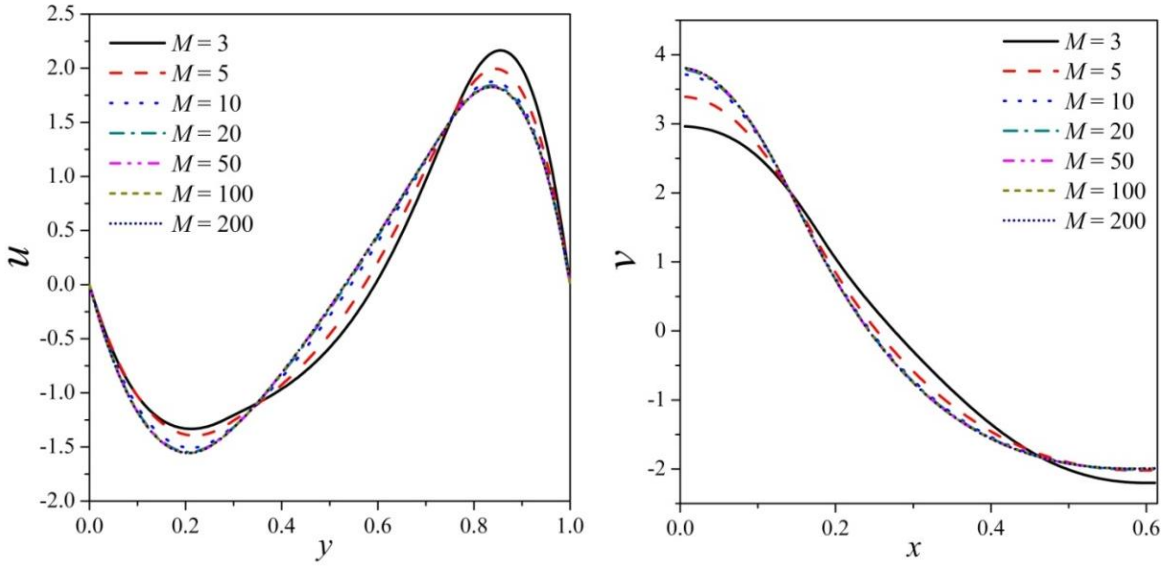

(a) (b)

Fig. 7 Velocity profiles for $T = 190$ and various values of *M*: (a) longitudinal velocity profile along $x = 0.307$, (b) vertical velocity profile along $y = 0.5$.

Table 2. Comparison of the maximum vertical velocity (*Vmax*), angular momentum (*AM*) and the electric Nusselt number (*Ne*) for T=190 and various values of *M*.

M	3	5	10	20	50	100	200
Vmax	3.146	3.520	3.755	3.807	3.822	3.823	3.824
AM	0.228	0.227	0.232	0.234	0.234	0.234	0.234
Ne	1.492	1.497	1.535	1.548	1.552	1.552	1.552

The reason for the dependency of the flow structure on *M* relates to the balance between the two terms ($M^2\left[q\vec{E}+\Delta\vec{u}/T\right]$ and $(\vec{u}\cdot\nabla)\vec{u}$) in the momentum equations [18]. For high *M*, the term $M^2\left[q\vec{E}+\Delta\vec{u}/T\right]$ is much stronger than $(\vec{u}\cdot\nabla)\vec{u}$, which means the inertial effects are fully

dominated. However, for lower values of M, it is not the case. Since the maximum velocity and charge void region are closely related to the subcritical bifurcation, it is logical to conjecture that the finite amplitude criterion T_f may also be M-dependent. In the next section, we will determine the finite amplitude criterion for various values of M.

Table 3. Numerical predictions of the linear stability criterion T_c for various values of M.

M	3	5	10	20	50	100	200
T_c	163.5	163.6	163.7	163.8	163.9	163.9	163.9

To close this subsection, we have provided in Table 3 values of T_c obtained from our simulations with various values of M. The method used to determine T_c is the same as other numerical studies, for example [8,18-20,26,28]. All these values should be compared with $T_c^a = 164.1$. The maximum difference between our numerical values and the analytical one is 0.37%, which shows a very good agreement.

4.2 Finite amplitude instability

Starting from a steady convection, we gradually decrease T and observe that the strength of flow motion also gradually decreases until a critical value, at which the motion suddenly stops. This critical value is smaller than the linear stability criterion, and it corresponds to the finite amplitude stability criteria T_f. For C=10, the nonlinear stability analysis predicted $T_f^a \approx 125.0$ for 2D rolls [10]. We recall that this value is predicted with the assumption that M is infinite (i.e. the inertial term is neglected) and the velocity field is approximated with only one mode.

In this study, we consider M varying in a wide range (M = 3, 5, 10, 20, 50, 100 and 200). In figure 8 the hysteresis loops which foreshadows the subcritical bifurcation is displayed for M=10.

The obtained T_f for this M value is 108.2. Here the bifurcation diagram used Vmax rather than Ne is to highlight the fact that Vmax is always higher than 1.0 in the range [T_f, T_c].

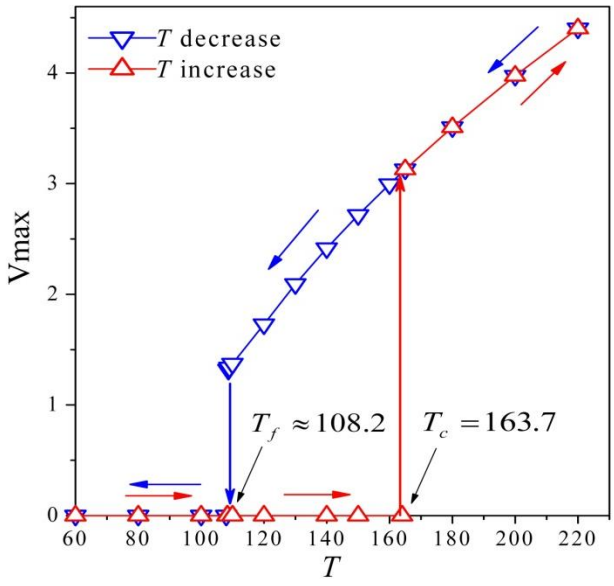

Fig. 8 Hysteresis loops respresented by the velocity amplitude Vmax for M = 10.

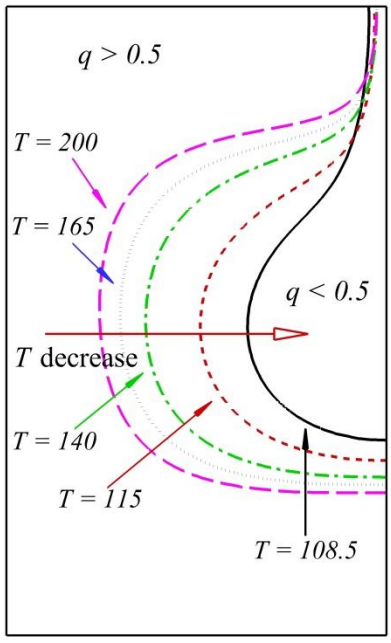

Fig. 9 Charge void region versus electric Rayleigh number, M = 10.

In figure 9, we have showed the variation of charge void region represented by the area of q<0.5 along with the decreasing T. By starting with a steady convection obtained with T=200 and gradually decreasing T, we observe the shrinking of the charge void region, which is explained by the smaller velocity amplitude with smaller T value [20]. We also observe that the area of void region does not decrease gradually to zero as closer to T_f but suddendly jumps from a non-zero value to a zero one. In other words, this area keeps a non-zero value for a T slightly above T_f ; see the separatrix curve for T = 108.5 in figure 9. This is because the electric torque is proportional to the area of the void region [1]. Therefore, in order to sustain a finite value of the fluid velocity, a finite area of the void region is needed.

Table 4. Estimated finite amplitude stability criteria T_f for various values of M.

M	3	5	10	20	50	100	200
T_f	105.0	107.0	108.2	108.8	109.0	109.0	109.0

For M = 3, 5, 20, 50, 100 and 200, the different flows follow a similar route as displayed in figure 9 from the convective state to still. The difference lies in the T_f value, at which the flow returns back to the rest state. In Table 4, we have summarized values of T_f stemming from our simulations for different values of M. Two situations arise: for $M > 20$, T_f takes almost a constant value, independent on M. For $M \leq 20$, T_f became M-dependent and T_f decreases with M. It should be noted that the numerical prediction of T_f is very sensitive to the numerical diffusion introduced when solving the hyperbolic charge transport equation [8,18,19]. To avoid any possible loss of accuracy, all results in Table 4 were computed with a very fine non-uniform grid with 160×320 control volumes, which guarantees the grid independency. Our present results are generally consistent with previous numerical predictions in [18,22,26,28]. Now it is clear that the discrepancy showed in Table 1 is partly because of the $T_f - M$ relationship.

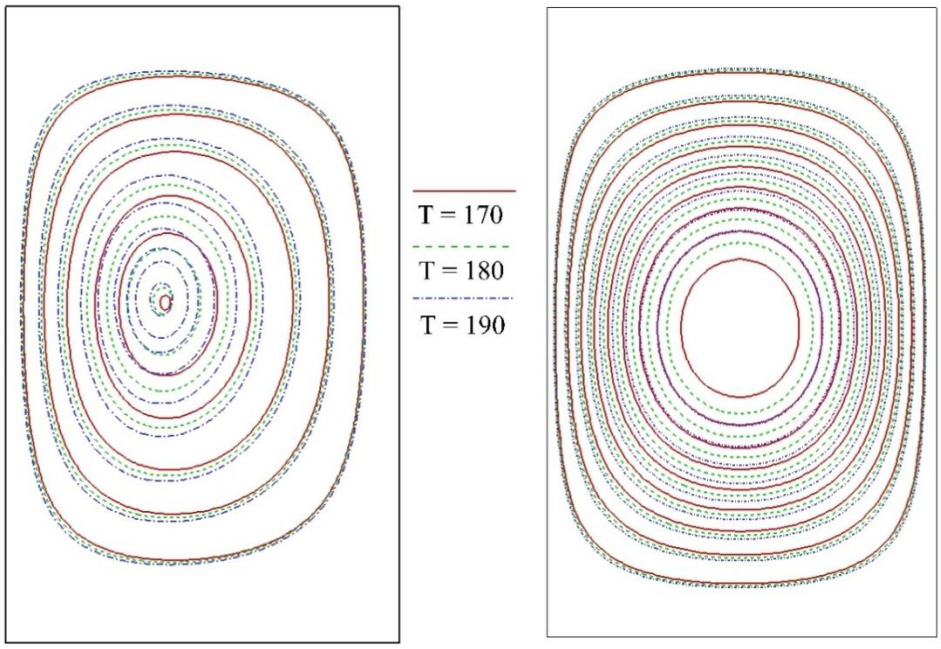

(a) (b)

Fig. 10 Stream functions with M = 10 and different values of T: (a) not exactly self-similar results obtained by solving all governing equations and (b) strongly self-similar results obtained by the imposed velocity field method with one mode.

We notice that there is a certain discrepancy between our numerical predictions of T_f and the analytical value of 125 predicted by the nonlinear stability analysis using one mode [10]. The discrepancy is due to the modal expansion used in the stability analysis. It is assumed to be self-similar, and it is unable to reproduce the sophisticated structure of the velocity field and the distribution of electric charge. The real flow structure, obtained from solving all the governing equations, is not exactly self-similar for different values of T, i.e. the streamlines do not superimpose exactly, see figure 10a. While strong self-similar flow structures are always observed in results obtained with the IVF method based on the modal expansion of velocity fields, see figure 10b. As discussed in [10], the presence of steep gradient in the charge density distribution with a certain amount of charge trapped in the void region is very difficult to reproduce with an expansion built with smooth functions.

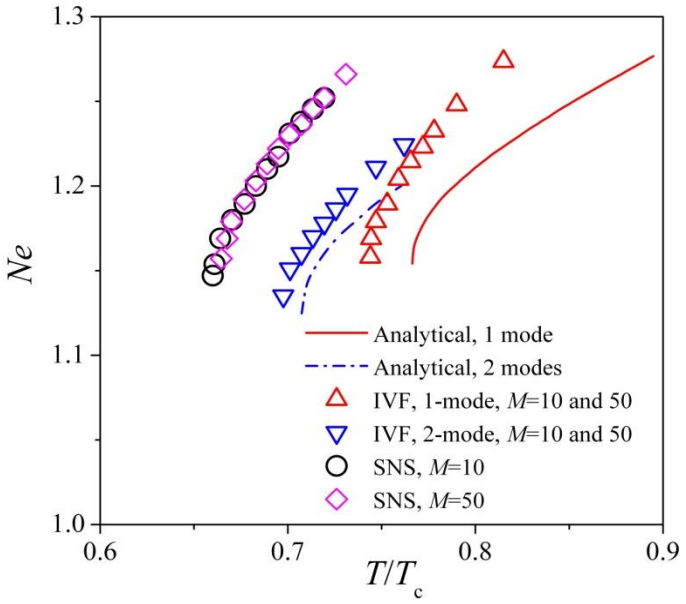

Fig. 11 Electric Nusselt number *Ne* as a function of T/T_c. The analytical curves are taken from [10].

In this study, we also determine the finite amplitude criterion using the IVF method based on the same velocity field expressions as the nonlinear stability analysis. The calculation procedure of the IVF method is well documented in [18,20]. The one-mode and two-mode expressions employed here for the velocity field are the same as the ones used in the stability analysis. The results are summarized in figure 11, in which the analytical curves are adopted from [10]. Our numerical results with the SNS approach are also presented for comparison. With the IVF method, the obtained T_f are 120.4 and 114.0 for cases of one-mode and two-mode, respectively. Both of them are close to the analytical values of 125 (one-mode) and 116 (two-mode). In [20], Chicón et al. found a value of T_f = 121.4 for the one-mode case, which is consistent with our finding. Slight difference may be due to the fluctuations in their charge density and velocity fields. These fluctuations were introduced by the PIC method used to treat the charge density equation, and they decreased the effective area of the void region and hence the driving electric torque [8]. Comparing to the one-mode approximation, the velocity field expressed with two modes are

closer to the real flow field. This explains why the T_f value obtained with the two-mode expression is closer to the one obtained by the SNS approach.

4.3 Characterization of a new subcritical bifurcation

To obtain a more complete picture of the flow bifurcation, we further increase the electric Rayleigh numbers. For another critical value of T, referred as T_{c2}, a new transition occurs where the flow transits from one convective cell to two cells. The new regime has already been observed by different researchers with different values of M [24,25,26,28,29]. The critical value T_{c2} that corresponds to the onset of the two-roll structure has been numerically determined in the range between 290 and 300 [29].

The same phenomenon has been confirmed in the present study for a wide range of M ($M \geq 10$). Figure 12 plots the time evolution of Vmax for $T = 420$ for various values of M. For all cases the flows first experience a one cell pattern similar to figure 5b, and then after a transition phase, a steady two-cell pattern with lower values of Vmax arises. Figure 13 displays the charge density distribution, stream function and the stream traces of charges to show the flow strucutre. The two counter-rotating rolls are highly symmetrical. When T is further increased, the two rolls start to oscillate periodically [26]. We have also performed the numerical experiments for the case of $M < 10$. However, the system doesn't show the same transition of flow structure as $M \geq 10$. Instead, the motion directly transits from the one-cell structure to an unsteady pattern at high values of T. This behavior may be due to the dual roles of M: the stabilizing role showing through the viscous coefficient T/M^2 and the destabilizing role with the driving term $M^2 q\vec{E}$; see Eqn. (2).

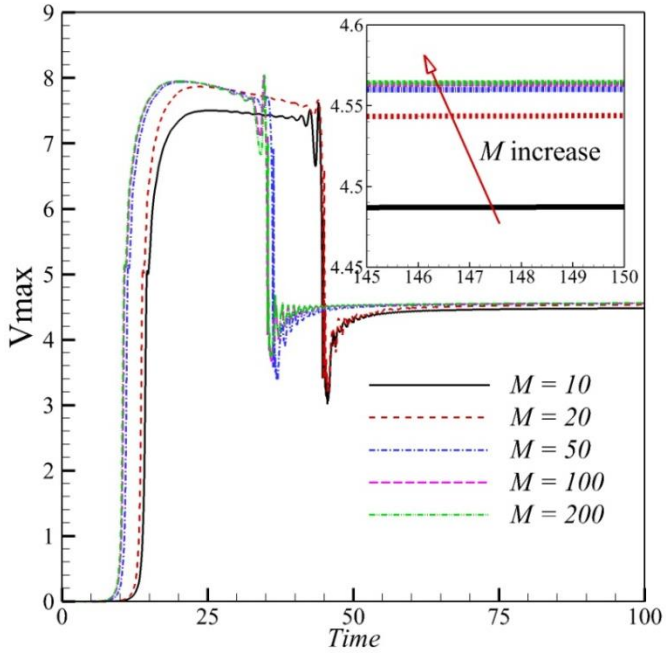

Fig. 12 Time evolutions of the maximum velocity for T = 420 for various values of M.

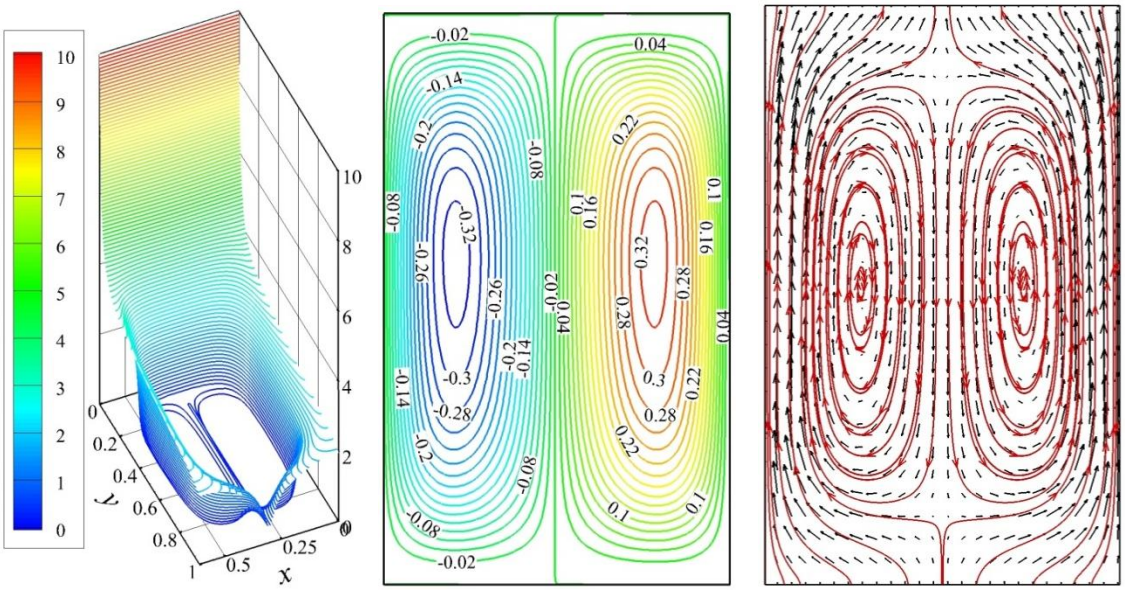

(a) (b) (c)

Fig. 13 Steady convection for T = 420 and M = 10. Iso-contours of (a) charge density and (b) stream function, (c) vectors and stream traces based on the full convective velocity $\vec{\omega}u+\vec{\omega}E$.

Previous studies have mainly focused on the description of the new flow structure. To deepen the study, we addressed the existence of a new subcritical bifurcation behavior with a new criterion T_{f2} reported in figure 14 and 15. The route of bifurcation when decreasing T from a value higher than T_{c2} is multiple. As shown in figure 14, restarting the computation from the previous state obtained for T = 480, but with lower T values will produce three different possible scenarios. The flow would keep a two-roll structure but with weaker velocity amplitude and smaller area of the charge void region if $T > T_{f2}$ (=192.1); see the curve of T = 195 in figure 14. If T_c (=164.1) < T < T_{f2}, the flow motion (two cells) will jump to rest at first, and then it will restart again but with one cell, which is due to the loss of the linear instability; see the curve of T = 190 in figure 14. If $T < T_c$ the flow will return and keep still; see the curve of T = 160 in figure 14.

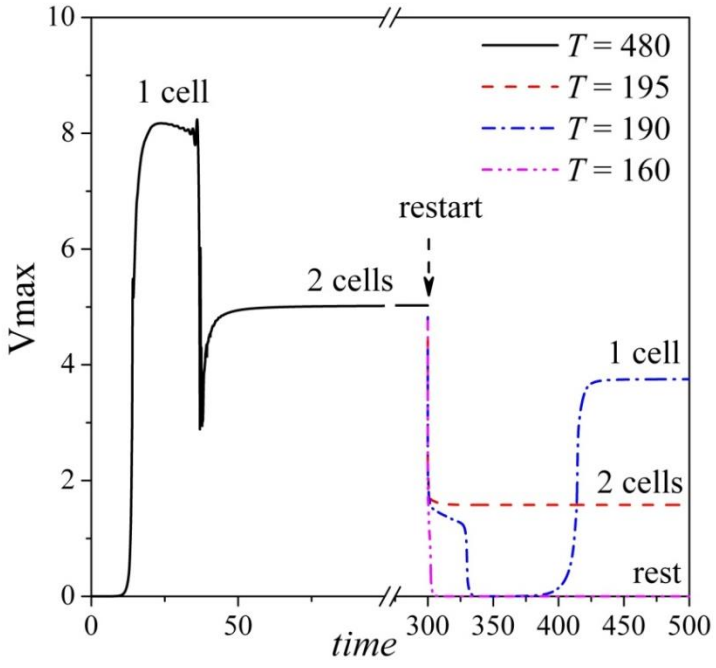

Fig. 14 Temporal evolution of the maximum velocity, M = 10.

The complete bifurcation diagram was summarized in figure 15. It's worth pointing out that both values of V_{max} at T_f and T_{f2} are higher than 1.0. This is consistent with the very basic

assumption for electro-convection, which states that the maximum velocity must be higher than the ionic velocity for a stable convection at least with free walls [9].

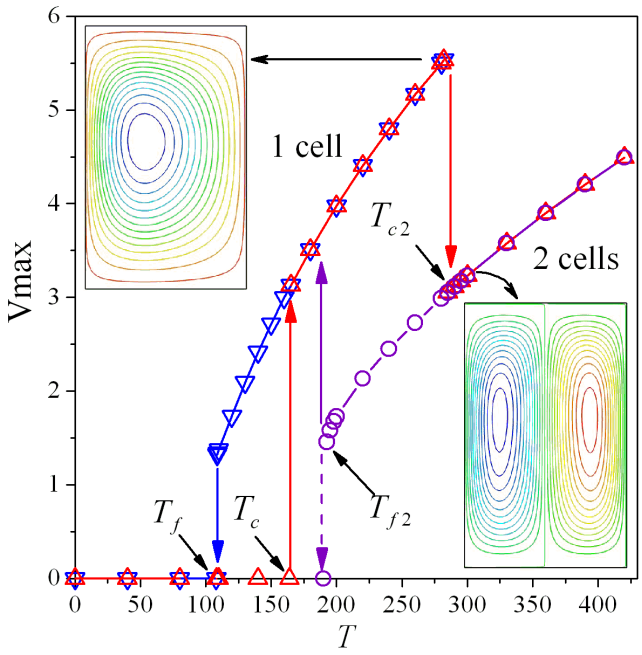

Fig. 15 Bifurcation diagram for $M = 10$. The nonlinear criteria are $T_f = 108.2$ and $T_{f2} = 192.1$.

We also investigate the influence of M on the new stability criterion T_{f2}, see table 5. It seems that T_{f2} is almost constant for all values of M considered, which is consistent with the results reported in table 3.

Table 5. The second nonlinear stability criteria T_{f2} for various values of M.

M	10	20	50	100	200
T_{f2}	192.1	192.2	192.2	192.2	192.2

5. CONCLUSIONS

In this paper, we performed a two-dimensional numerical investigation of the electro-convection induced by a strong unipolar injection of ions in a plane layer of dielectric liquid. The system is characterized by a subcritical bifurcation in the finite amplitude regime. By combining

the numerical results, we first analyzed the formation process of the flow motion and the void region of charges. Then we accurately determined both the linear stability criterion (T_{c1}) and the finite amplitude one (T_{f1}) for various values of the mobility parameter M. It is found that both the flow structure and T_{f1} are M-dependent for $M \leq 20$. For $M > 20$, T_{f1} takes a constant value. This finding highlights the fact that T_{f1} is unlike T_{c1} as it heavily depends on the flow structure and charge density distribution. In addition, we noticed a certain discrepancy of T_{f1} between our numerical values and the ones predicted by the stability analysis. This is due to the simple modal expansion for the velocity field used in the stability analysis, which is not sufficient to guarantee an accurate description of the real velocity and charge density distributions in such Coulomb-driven flows. Our present findings concerning the finite amplitude criterion can serve as the reference results for code validation.

By extending the electric Rayleigh number T to higher values, the system shows a transition of the flow structure from one convective cell to two cells. We find that such a transition is also featured by a subcritical bifurcation with two new criteria T_{c2} and $T_{f2,}$ which correspond to the onset and stop of the two-cell structure, respectively. A complete bifurcation diagram for the finite amplitude regime is finally obtained.

ACKNOWLEDGMENTS

This work was partially funded by the French Government program “Investissements d’Avenir” (LABEX INTERACTIFS, reference ANR-11-LABX-0017-01) (to Jian Wu), a grant of the French district Poitou- Charentes (to P. Traoré), and partially by financial support from the Spanish Ministerio de Cienciay Tecnología (MCYT) under Research Project No. FIS2011-25161 and Junta de Andalucía under research projects P10-FQM-5735 and P09-FQM-4584 (to A. T. Pérez). Jian Wu thanks Mengqi Zhang of Université de Poitiers for his fruitful discussion.

REFERENCES

[1] Castellanos A, “Coulomb driven convection in electrohydrodynamics”, IEEE Transactions on Dielectrics and Electrical Insulation, vol. 26, pp. 1201-1215, 1991.

[2] Atten P, “Electrohydrodynamic instability and motion induced by injected space charge in insulating liquids”, IEEE Transactions on Dielectrics and Electrical Insulation, vol.3, pp. 1-17, 1996.

[3] Denat A, Gosse B, Gosse J P, “Ion injections in hydrocarbons”, Journal of Electrostatics, vol. 7 pp. 205-225, 1979.

[4] Jones B. T., “Electrohydrodynamically enhanced heat transfer in liquids - A review”, Advances in Heat Transfer, vol. 14, pp. 107-148, 1978.

[5] Seyed-Yagoobi J, Bryan E J, “Enhancement of heat transfer and mass transport in single-phase and two-phase flows with electrohydrodynamics”, Advances in Heat Transfer, vol. 33, pp. 95-186, 1999.

[6] McCluskey F M J, Atten P, “Modifications to the wake of a wire across Poiseuille flow due to a unipolar space charge”, Journal of Fluid Mechanics, vol. 197, pp. 81-104, 1988.

[7] Atten P, Moreau R, “Stabilité electrohydrodynamique des liquids isolants soumis a une injection unipolaire”, Journal de Méchanique, vol. 11, pp. 471-520, 1972.

[8] Castellanos A, Atten P, Pérez A T, “Finite amplitude electroconvection in liquid in the case of weak unipolar injection”, CH PhysicoChemical Hydrodynamics, vol. 9 (3/4), pp. 443-452, 1987.

[9] Felici N, “Phénomènes hydro et aérodynamiques dans la conduction des diélectriques fluids”, Revue Générale de l’Electricité vol. 78, pp. 717-734, 1969.

[10] Atten P, Lacroix J C, “Non-linear hydrodynamic stability of liquids subjected to unipolar injection”, Journal de Mécanique, vol. 18, pp. 469-510, 1979.

[11] Watson P K, Schneider J M, Till H R, “Electrohydrodynamic stability of Space-charge-limited currents in dielectric liquids II. Experimental study”, Physics of Fluids, vol. 13, pp. 1955-1964, 1970.

[12] Lacroix J C, Atten P, Hopfinger E J, “Electroconvection in a dielectric layer subjected to unipolar injection”, Journal of Fluid Mechanics, vol. 69, pp. 539-563,1975.

[13] Atten P, Lacroix J C, “Electrohydrodynamic stability of liquids subjected to unipolar injection: non linear phenomena”, Journal of Electrostatics, vol.5 pp. 439-452, 1978.

[14] Castellanos A, Pérez A T, Chicon R, “Chaotic electroconvection in a layer of dielectric liquid subjected to unipolar injection: Maximal Lyapunov exponents”, International Journal of Bifurcation and Chaos, vol. 12(11), pp. 2523-2534, 2002.

[15] Suh Y K, “Modeling and simulation of ion transport in dielectric liquids-Fundamentals and review”, IEEE Transactions on Dielectrics and Electrical Insulation, vol. 19(3), pp. 831-848, 2012.

[16] Adamiak K, “Numerical models in simulating wire-plate electrostatic precipitators: a review”, Journal of Electrostatics, vol. 71, pp. 637-680, 2013.

[17] Pérez A T, Castellanos A, “Role of charge diffusion in finite-amplitude electro-convection”, Physical Review A, vol. 40(10), 5844, 1989.

[18] Traoré P, Jian W, “On the limitation of imposed velocity field strategy for Coulomb-driven electroconvection flow simulations”, Journal of Fluid Mechanics, vol. 727, R3, 2013.

[19] Castellanos A, Atten P, “Numerical modeling of finite amplitude convection of liquids subjected to unipolar injection”, IEEE Transactions on Industry Applications, vol. IA-23, pp. 825-830, 1987.

[20] Chicón R, Castellanos A, Martín E “Numerical modelling of Coulomb-driven convection in insulating liquids”, Journal of Fluid Mechanics, vol. 344, pp. 43-66, 1997.

[21] Vázquez P A, Georghiou G E, Castellanos A, “Characterization of injection instabilities in electrohydrodynamics by numerical modelling: comparison of particle in cell and flux corrected transport methods for electroconvection between two plates”, Journal of Physics D: Applied Physics, vol. 39, pp. 2754-2763, 2006.

[22] Cerizza D, "Electroconvection in three dimensions: a numerical study", Master Thesis, Politecnico di Milano, Italy, 2007.

[23] Luchini P, Quadrio M, "A low-cost parallel implementation of direct numerical simulation of wall turbulence", Journal of Computational Physics, vol. 211(2), pp. 551-571, 2006.

[24] Vázquez P A, Georghiou G E, Castellanos A, "Numerical analysis of the stability of the electrohydrodynamic (EHD) electroconvection between two plates", Journal of Physics D: Applied Physics, vol. 41, pp. 175303-175313, 2008.

[25] Kourmatzis A, Shrimpton J S, "Turbulent three-dimensional dielectric electro-hydrodynamic convection between two plates", Journal of Fluid Mechanics, vol. 696, pp. 228-262, 2012.

[26] Traoré P, Pérez A T, "Two-dimensional numerical analysis of electroconvection in a dielectric liquid subjected to strong unipolar injection", Physics of Fluid, vol.24 (3), pp. 037102, 2012.

[27] Harten A, "High resolution schemes for hyperbolic conservation laws", Journal of Computational Physics, vol. 49(3), pp. 357-393, 1983.

[28] Vázquez P A, Castellanos A, "Numerical simulation of EHD flows using Discontinuous Galerkin Finite Element methods", Computers & Fluids, vol. 84, pp. 270-278, 2013.

[29] Wu J., Traoré P, Fang-Bao T, Pérez A T, Louste C, Dascalescu L, "Effect of mobility parameter on the oscillatory electro-convection of dielectric liquids subject to strong unipolar charge injection", IEEE Transactions on Industry Applications, vol. 50(4), pp. 2306-2313, 2014.

[30] Castellanos A, "Electrohydrodynamics", Springer Verlag Autriche, 1998.

[31] Shrimpton J, "Charge Injection Systems: Physical Principles, Experimental and Theoretical Work", Springer, 2009.

[32] Ferziger J H, Perić M, "Computational methods for fluid dynamics", 3rd edition, Berlin: Springer, 2002.

[33] Patankar S V, Spalding D B, “A calculation procedure for heat, mass and momentum transfer in three-dimensional parabolic flows”, International Journal of Heat and Mass Transfer, vol. 15(10), pp. 1787-1806, 1972.

[34] Rhie C M, Chow W L, “Numerical study of the turbulent flow past an airfoil with trailing edge separation”, AIAA Journal, vol. 21(11), pp. 1525-1532, 1983.

[35] Gaskell P H, Lau A K C, “Curvature-compensated convective transport: SMART, A new boundedness-preserving transport algorithm”, International Journal for Numerical Methods in Fluids, vol. 8(6), pp. 617-641, 1988.

[36] Waterson N P, Deconinck H, “Design principles for bounded higher-order convection schemes – a unified approach”, Journal of Computational Physics, vol. 224(1), pp. 182-207, 2007.

[37] Jian W, Traoré P, Louste C, “An efficient finite volume method for electric field-space charge coupled problems”, Journal of Electrostatics, vol. 71(3), pp. 319-325. 2013.

[38] LeVeque R J, “Finite volume methods for hyperbolic problems”, Cambridge university press, pp.130-132, 2002.

[39] Atten P, Lacroix J C, Malraison B, “Chaotic motion in a Coulomb force driven instability: Large aspect ratio experiments”, Physics Letters A, vol. 79, pp.255-258, 1980.

[40] Malraison B, Atten P, “Chaotic behavior of instability due to unipolar ion injection in a dielectric liquid”, Physical Review Letters, vol. 49, pp. 723-726, 1982.

[41] Schneider J M, Watson P K, “Electrohydrodynamic stability of space‐charge‐limited currents in dielectric liquids. I. theoretical study”, Physics of Fluids, vol. 13(8), pp.1948-1954, 1970.

[42] Chacón R, “An analytical study of Hamiltonian chaos in nonsteady finite-amplitude electroconvection”, International Journal of Bifurcation and Chaos, vol. 24(02), pp. 1450019, 2014.